A study of dust structure nearby white dwarf WD1334-678

Ishwor Nath Joshi, Ajay Kumar Jha*, Binil Aryal

Central Department of Physics, Tribhuvan University, Kirtipur
*Email: ajay.jha@cdp.tu.edu.np

ABSTRACT

A low flux density region nearby white dwarf WD1334-678 in the 140 μm AKARI survey maps has been systematically searched and found a far-infrared cavity centerd at R.A. (J2000) = $13^h38^m14.4^s$, Dec.(J2000) = $-68°40'42"$, in which minimum flux is 19.5 MJy/sr at 90 μm wavelength. The physical properties (Size, dust color temperature, dust mass) and thermodynamic property (Planck function distribution) of the cavity using 140 μm and 90 μm AKARI survey data has been presented. The size of the cavity is found to be $0.17° \times 0.12°$. The dust color temperature is found in the range 17.70 ± 0.01 K to 18.81 ± 0.01 K. The Plank function distribution along major and minor diameters shows a very good agreement with sinusoidal fitting. The period of oscillation of dust particles along major and minor diameters are 3.2 $Wm^{-2}Sr^{-1}Hz^{-1}arcmin^{-1}$ and 1.6 $Wm^{-2}Sr^{-1}Hz^{-1}arcmin^{-1}$, respectively.

1. Introduction

The low and intermediate-mass (M < 10 M_o) stars formed by nuclear burning, appears as a red giant in the region of Hertzsprung-Russell diagram, is called Asymptotic Giant Branch (AGB) stars [1]. When an Asymptotic Giant Branch star exhausts the supply of hydrogen in its core, the core shrink and its temperature increases, causing the outer layers of the star to expand and cool. The star's luminosity increases, and it becomes a red giant, following a track leading into the upper right hand corner of the HR diagram (Blandford& Rees, 1974). The AGB phase is divided into two parts, the early AGB (E-AGB) and the thermally pulsing AGB

(TP-AGB). During the E-AGB phase the principal source of energy is helium fusion in a shell around a core consisting mostly of carbon and oxygen. During this phase the star swells up to giant proportions to become a red giant again. The star may become as large as one astronomical unit. After the helium shell runs out of fuel, the TP-AGB starts. Now the star derives its energy from fusion of hydrogen in a thin shell, inside of which lies in the now inactive helium shell. However, on periods of 10,000 to 100,000 years the helium shell switches on again, and the hydrogen shells switches of a process known as a helium shell ash [2].

Towards the end of their lifetime, almost all (95-98%) stars lose a substantial fraction of their mass

on the Asymptotic Giant Branch (AGB) in form of massive winds, which compels them into the Planetary Nebula (PN) phase. The central star of PN is the white dwarf. The massive stellar wind emitted from the AGB star interacts with the ambient interstellar medium. Thus the structure (gas or the dust) around the white dwarf preserve the history as a fossil record of the early and late AGB phase of the star. It is important to understand the shaping process of interstellar clouds as well as the nature of the emission from AGB to PN phase. The white dwarf is suspected to reside within giant dust structures which may represent fossil records of its progenitor's transition from spherically symmetric to bipolar or unipolar mass loss. It can be suspected that the white dwarf is not the only one where fossil records of ancient mass loss in its neighborhood as well as signs of the resulting shaping can be traced. Besides being ideal laboratories for the study of various astrophysical processes prevailing in highly excited dilute nebulae, PNe and their ancestors are key objects for the understanding of the evolution of stars. In this connection, the transformation from spherically symmetric AGB winds to non-spherical PNe represents one of the most enduring problems of stellar astrophysics [3]. The study regarding evolved planetary system around white dwarfs has produced a separate insight into the end state of planetary system and provided that the measurements of proportion of the extra-solar planets [4].

Kiss et al [5] and koenyves et al [6] investigated 462 far-infrared loops and studied their size, temperature luminosity. Wienberger and Armsdorfer discovered very large (9^0) jet like structures in the FIR (Far Infrared) suggest in the interaction of the wind of the Asymptotic Giant Branch (AGB) stars with ambient ISM matter [7]. Aryal et al [8] found two giant (2.1 pc, 0.9pc) bipolar dust emission structures centered on NGC1514. This is one of the very few known cases where the history of all main mass-loss phases of the intermediate initial mass star is preserved. Jha

& Aryal [9] performed the study of dust color distribution of two new cavity-like structures (sizes ~ 2.7pc × 0.8pc and ~ 1.8pc × 1pc) using IRAS and AKARI maps near Pulsars. They found the difference in the average temperature in IRAS and AKARI maps to be 3.2 ± 0.9K and 4.1 ± 1.2K. A larger value of dust color temperature was found in a longer wavelength AKARI map than in the IRAS map which is not normally possible. So, we are interested to study the physical properties of far infrared cavity nearby the white dwarf WD1334-678 in 90 and 140 μm AKARI which will give the clear hint of shaping mechanism of ISM.

2. Methods

We found a far-infrared cavity at 90 and 140 μm AKARI nearby white dwarf WD1334-678. We downloaded the FITS (Flexible Transport Image System) image of a cavity structure at 90 and 140 μm. We had processed it by using the software Aladin v2.5. Contours were drawn to separate the minimum flux region within the structure. The corresponding flux at 90 and 140 μm at each pixel were measured in the region of interest. Possible sources for the background flux were studied using the SIMBAD database (https://simbad.u-strasbg.fr/simbad/). We adopt the following methods for calculations of flux densities, dust color temperature, Planck's function a dust mass and size of cavity in the selected region nearby the white dwarf.

Dust color temperature

We adopt the method developed by Schnee et al [10] to determine the dust color temperature of dust. The flux density of emission at a wavelength λ_i is given by

$$F_i = \left[\frac{2hc}{\lambda_i^3 \left(e^{\frac{hc}{\lambda_i kT_d}} - 1 \right)} \right] N_d \alpha \lambda_i^{-\beta} \Omega_i \qquad (1)$$

where h is Planck's constant, k is Boltzmann's constant, c is the speed of light, N_d is the column density of dust grains, α is a constant which relates the Flux with the optical depth of the dust, β is the

spectral emissivity index and Ω_i is the solid angle subtended at λ_i by the detector.

We assumes $T_d \ll 1$ and $\Omega_{140} = \Omega_{90}$ and also $\lambda_{140} = \dfrac{hc}{KT_{140}}$ and $\lambda_{90} = \dfrac{hc}{KT_{90}}$, the ratio R of the Flux densities at 90 and 140 μm is given as

$$R = \frac{F(90\mu m)}{F(140\mu m)} = \left(\frac{90}{140}\right)^{-(3+\beta)}\left[\frac{e^{\frac{T_{140}}{T_d}}-1}{e^{\frac{T_{90}}{T_d}}-1}\right]\frac{\Omega_{90}}{\Omega_{140}} \qquad (2)$$

But $T_{140} = 103$ and $T_{90} = 160$ from equation (2) becomes

$$R = 0.64^{-(3+\beta)}\frac{e^{\frac{103}{T_d}}-1}{e^{\frac{160}{T_d}}-1} \qquad (3)$$

Following Dupac et al. [11], we use the equation,

$$\beta = \frac{1}{(\delta + \omega T_d)} \qquad (4)$$

to describe the observed inverse relationship between T_d and β. Here, δ and ω are free parameters found that the temperature dependence of the emissivity index fits very well with the hyperbolic approximating function. The value of β depends on dust grain properties as composition, size, and compactness. For reference, $\beta = 0$, 1 and 2 for pure blackbody, the amorphous layer-lattice matter and the metals and crystalline dielectrics respectively [12]. We used $\beta = 2$ for dust as suggested by Jha & Aryal (2017) [13]. For a smaller value of T_d, 1 can be dropped from both numerator and denominator of equation and it takes the form

$$R = 0.64^{-(3+\beta)}\cdot\frac{e^{\frac{103}{T_d}}}{e^{\frac{160}{T_d}}} \qquad (5)$$

Taking the natural logarithm on both sides of equation (5) we get,

$$\ln(R) = \ln 0.64^{-(3+\beta)}\left[\frac{103}{T_d} - \frac{160}{T_d}\right] = \ln 0.64^{-(3+\beta)}\left[\frac{-57}{T_d}\right] \qquad (6)$$

We find the expression for the temperature as,

$$T_d = \frac{-57}{\ln\left[R\times 0.64^{(3+\beta)}\right]}$$

where $R = \frac{F(90\mu m)}{F(140\mu m)}$ $\qquad (7)$

F(90 μm) & F(140 μm) are the flux densities at 90 μm and 140 μm, respectively. In this way, we can use equation (7) for the determination of the dust grain temperature [14].

Planck's function

The power emitted by a body as radiation of different frequencies per unit surface area of the body, per unit solid angle per unit frequency is termed as spectral radiance of that body. According to Planck, the spectral radiance of a body at frequency (ν) and temperature (T) is given by [15],

$$B(\nu, T) = \frac{2h\nu^3}{c^2}\left[\frac{1}{e^{\frac{h\nu}{k_B T}}-1}\right] \qquad (8)$$

This equation is called the expression for Planck's function

where,

k_B = Boltzmann's constant

c = Speed of light

ν = Frequency at which the emission is observed

h = Planck's constant

and

T = Dust color temperature of each pixel

By using the formula given by equation (8), we can calculate the Planck's function of each pixels of the cavity. We finally plot graphs of Planck's function versus distance along the major and minor axes to study the distribution of Planck's function along the extension and compression of the cavity. The value of Planck's function depends on the wavelength (frequency) and temperature [16]. The mass of the dust within the region of interest can be calculated by the method of Hildebrand (1983) [17].

3. Results and Discussion

Structure: Contour map

For the systematic search on AKARI maps, the white dwarf WD1334-678 is located at R.A. (J2000) = 13^{h}38^{m}14.4^s, Dec. (J2000) = −68°40'42". The size of the cavity found nearby the White Dwarf is 0.17°× 0.12°. Using the ALADIN v2.5 suitable contours are made at level 1 and 50 that enclose the minimum flux density of the isolated cavity. The

contour map of cavity the contour level 1 to 50 at 140μm as shown in figure 1 (a).

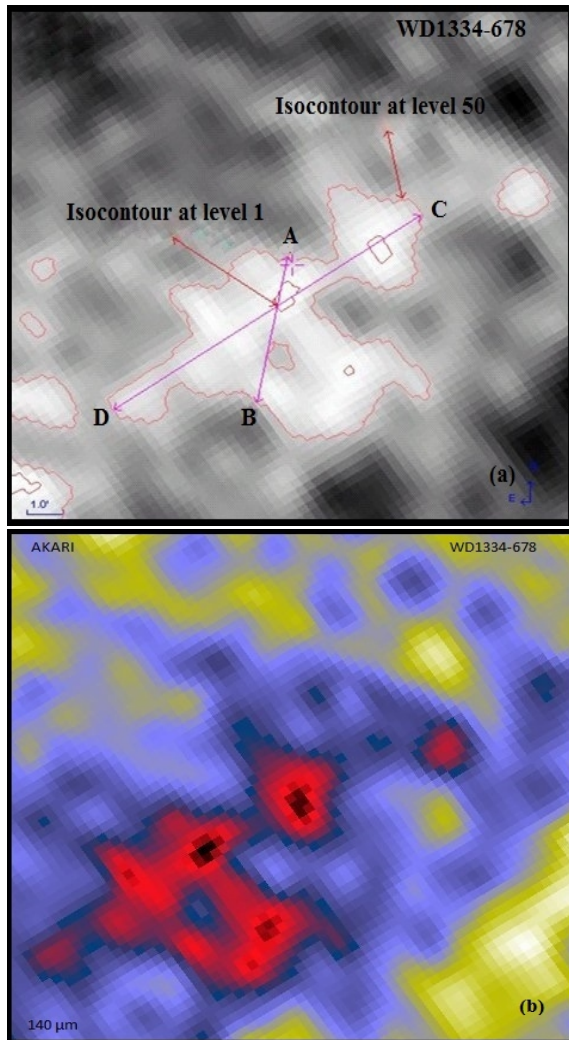**Fig. 1:** (a) Showing contour levels in FITS image of far-infrared cavity nearby WD1334-678 at 140 μm. Two contours at 140 μm image for the best selection of contour with major axis CD and minor axis AB and (b) JPEG image of WD1334-678 at 140 μm [18].

Distribution of flux density and contour map at 140 μm

The values of AKARI flux densities at 90 μm and 140 μm have measured using ALADIN2.5 software. Figure2 (a) shows graph between flux at 90 μm and 140 μm. A best fit straight line is drawn on the data. The slope of the line is 0.035. Using equation (7) and values of the slope of best fit line, we calculated the dust color temperature. Inside the cavity, the dust color temperature found to be varied from 17.70 ± 0.01 K to 18.81 ± 0.01 K. For the minimum and maximum fluxes, no good correlation is seen whereas for the intermediate flux values, there is good correlation.

Fig 2 (b) shows the AKARI 140 μm far infrared image of the core region of the cavity located nearby white dwarf WD1334-678 having size $0.17° \times 0.12°$ at R.A. (J2000) = 13^h38^m 14.4^s, Dec. (J2000) = $-68°40'42"$. We got different contours levels by plotting the flux densities at 140 μm. The contour levels are at fluxes 46.14, 49.02, 51.90, and 53.82MJy/sr respectively. From Fig. 2 (b), we can see that the gap between two counter levels at northern-east region is very small, while the gaps between counter levels become broaden at southern-west region. There may be external sources in northern-east region so that that the counter levels at northern region are compressed. This indicates that mass loading takes place in the middle part of the cavity.

Contour maps of dust color temperature and dust mass distribution

Fig.3a and 3b represent the dust color temperature and dust mass contour maps. From Fig. 3a, in southern-east, low temperature can be seen, while higher mass can be seen in this region (Fig. 3b). Similarly, along north-east temperature is high, while the mass is low. It is seen that the lower the temperature higher the mass in the contour maps which is expected trend. In the core region, higher mass distribution can be seen (Fig. 3b) but in that region, temperature is not low. This shows that there might be an external cause. Dust mass contour map and dust color temperature contour map gives the information of the distribution of the dust mass and dust color temperature within the region of interest respectively.

Gaussian nature of dust color temperature and dust mass

Fig.4a and 4b represent the Gaussian temperature and the Gaussian mass distributions respectively. The value of standard deviation is found to be (σ) = 0.21 and mean value is (x_c) = 18.15 K. Since the standard deviation is small, we can expect that the data values tend to be close to the mean value of the temperature i.e. small variation of data values from mean can be expected. From fig.4a, it is clear that the data are skewed right. This implies that the temperature distribution is not quite symmetric. The Gaussian distribution curve is left skewed in Fig. 4b. This suggests that the mass distribution has lack of perfect symmetry.

The average value of the dust color temperature in the core region of the cavity is found to be 18.15 K, equal to the Gaussian center (Fig.4a) with an offset of 1.10 K (< 2 K), suggests that the cavity is dynamically stable [19]. Generally, the Gaussian distribution is found to be in the good agreement with both T_d and M_d distributions (Figs. 4a, b). However, Gaussian width and skewness are found to be different in these plots, suggesting an external effect, probably from any wind blowing objects.

Distribution of Planck's function along the extension and compression of the cavity

Fig. 5a and 5b represent the variation of Planck's function along major and minor diameter of the cavity respectively. The solid curve stand for the sinusoidal plot, Fig. (5 a,b) clearly shows that the Planck's function first decreases along with distance for the major diameter. It goes down to a certain minimum value 1.42×10^{-16} and then increases with the distance. The fluctuation of Planck's function with distance frequently implies the instability inside the cavity which is responsible for the violation of the thermodynamic equilibrium. This might tell us the presence of effect of wind blower inside the cavity.

But in case of minor diameter, the Planck's function increases slightly and then decreases with the distance. Here the materials are in the local thermodynamic equilibrium along the compression (minor diameter) of the cavity. So, this variation seems to make our cavity is isolated and stable.
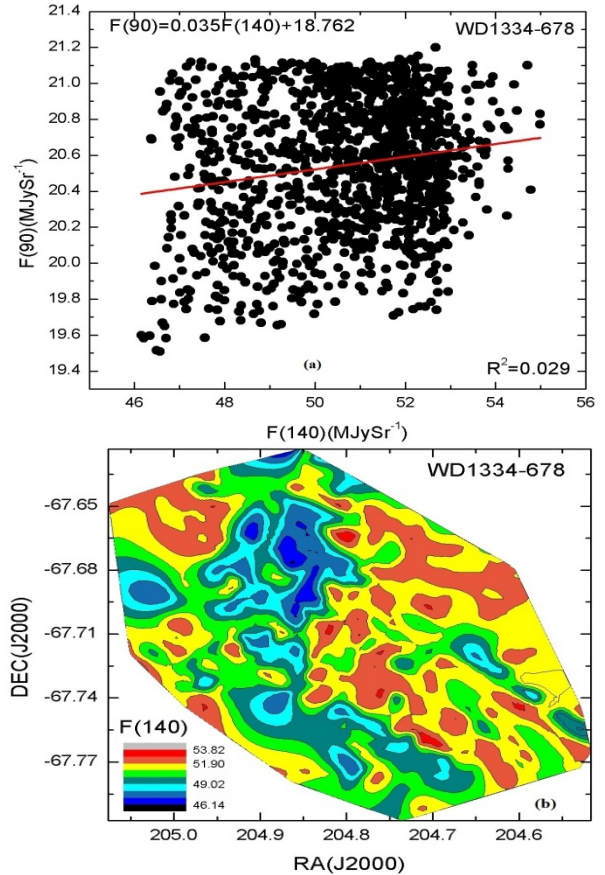

Fig. 2: (a) Flux density at 90 μm versus 140 μm plot. The solid line represents the best fitted line. The best fitted line and the regression coefficient are given. The R^2 value and the distribution of data suggests that there is no correlation between 90 and 140 μm fluxes in the far-infrared cavity. This suggests that this cavity might not be formed naturally and (b) AKARI 140 μm far infrared images of the core region of White Dwarf cavity WD1334-678 centered at R.A. (J2000) = $13^h38^m14.4^s$, Dec. (J2000) = −68°40'42". The color bars are given for flux density in MJy/Sr..

The Planck's function of dusts found to obey sinusoidal variation along extension given by

$$B\ (\nu,T) = 1.656\times10^{-16} + 1.697\times10^{-17} \cdot \sin[\ \pi\frac{(x-3.289)}{3.227}\ ]$$

$$(10)$$

Similarly, for minor diameter Planck's function distribution is shown in Fig. 5b.

Along the compression (minor diameter), best fit sinusoidal curve obey the equation (11)

$$B\ (\nu,T) = (1.592\times10^{-16}) + (1.374\times10^{-17})\cdot\sin[\pi\frac{(x-0.861)}{1.691}]$$

$$(11)$$

From figures 5a and 5b, it can be concluded that dust particles are oscillating sinusodially along extension and compression with periods 3.2 $Wm^{-2}Sr^{-1}Hz^{-1}arcmin^{-1}$ and 1.6 $Wm^{-2}Sr^{-1}Hz^{-1}arcmin^{-1}$, respectively.

Fig. 4: The distribution of dust color temperature (a) and dust mass (b). The solid curve represents Gaussian fits. The Gaussian parameters are given. The error bar represents ±1σ of the deviation.

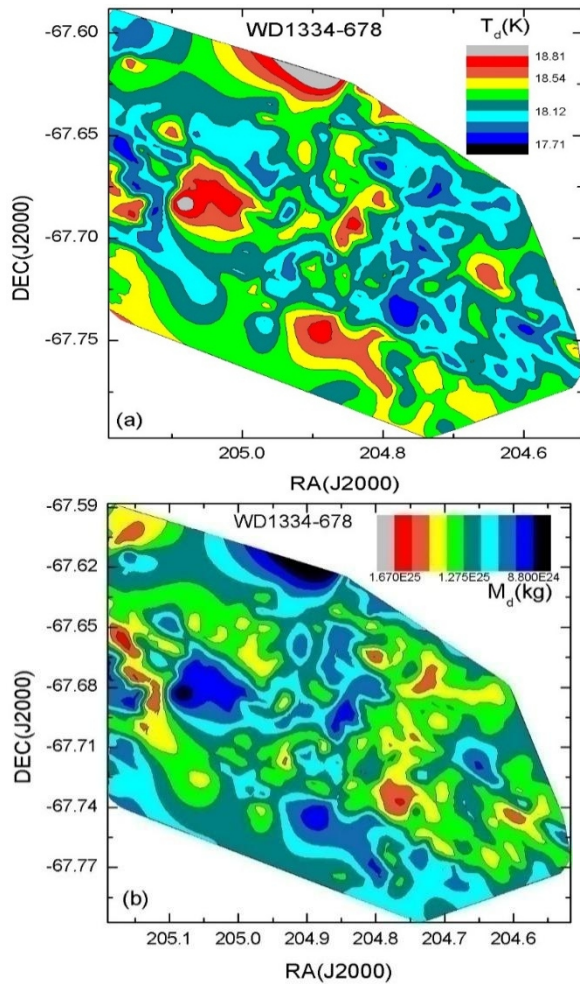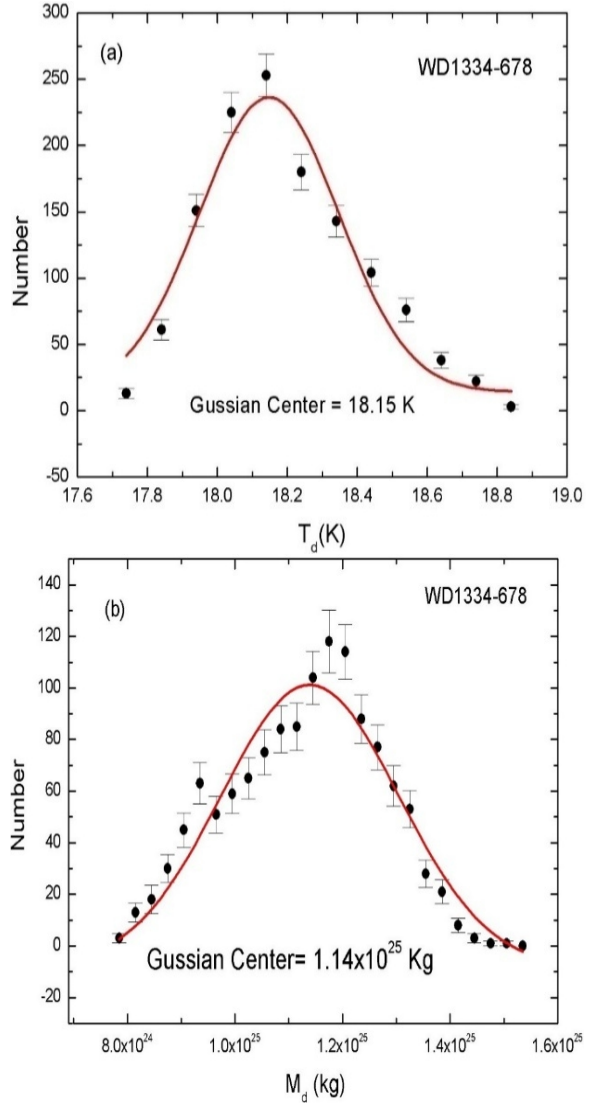**Fig. 3:** The contour map of dust Color temperature (a) and dust mass (b). The contour levels are shown.
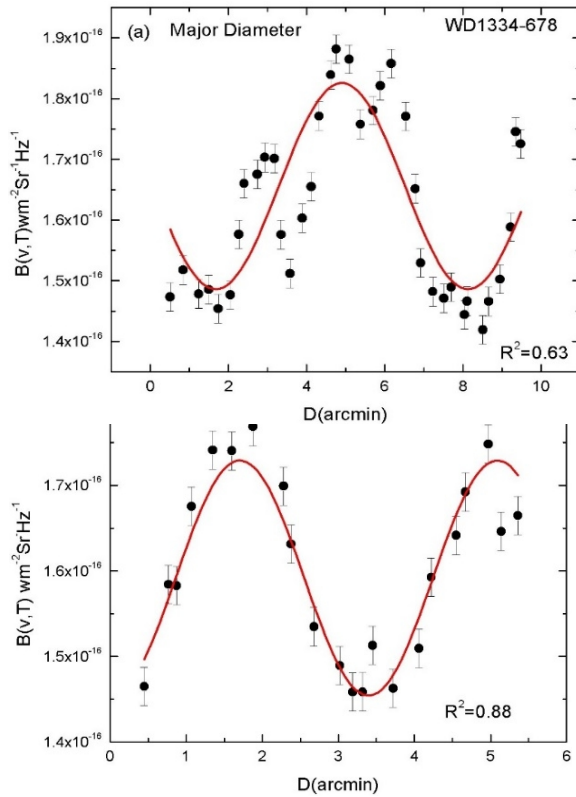
Fig. 5: Variation of Planck's function with distance along the major (a) and minor (b) diameter of the cavity. The solid lines represent sinusoidal fit. The error bar is the standard error of the deviation.

4. Conclusion

We systematically searched a far infrared cavity nearby White Dwarf WD1334-678 in AKARI maps centered at R.A. (J2000) = $13^h38^m14.4^s$, Dec. (J2000) $=-68°40'42''$. We studied physical (size, dust color temperature, dust mass) and dynamic (Planck function distribution) properties of the cavity. We conclude our results as follows:

(a) The size of the far infrared cavity is found to be $0.17°\times 0.12°$. The minimum flux density at 140μm is found to be 46 MJy/sr. The dust color temperature is found to lie in the range 17.70 ± 0.01 K to 18.81 ± 0.01 K.

(b) The average mass of the dust in the cavity is found to be 1.1×10^{25} kg. It indicates that the region

is mass deficiency region, suggest the external cause (White Dwarf). The White Dwarf (WD1334-678) might have blown and swept away the material from the region of cavity.

(c) The Planck function distribution along the major and minor diameter of the cavity showed non-uniform distribution, suggesting that the dust in the cavity are not in the thermodynamically equilibrium.

(d) Planck function distribution show sinusoidal nature. This indicates that the dust in the cavity might be oscillating in order to gain stability. The period of oscillation along extension (major diameter) and compression (minor diameter) are found to be 3.2 $Wm^{-2}Sr^{-1}Hz^{-1}arcmin^{-1}$ and 1.6 $Wm^{-2}Sr^{-1}Hz^{-1}arcmin^{-1}$, respectively.

References

[1] F. Herwig, Evolution of Asymptotic Giant Branch Stars, Annual Review of Astronomy and Astrophysics 43 (2005) 435-479. https://doi.org/10.1146/annurev.astro.43.072103.150600

[2] B. Aryal and R. Weinberger, Dust Structure Around White Dwarf WD1003-44 in 60 & 100 μm Iras Survey, Himalayan Physics 2 (2011) 5-10. https://doi.org/10.3126/hj.v2i2.5202

[3] B. Aryal, Asymmetric Mass-loss from the White Dwarf WD 0253+209: Secret Revealed, BIBECHANA 8 (2012) 1-7. https://doi.org/10.3126/bibechana.v8i0.4806

[4] D. Koester, B.T. Gansicke, J. Farihi, The Frequency of Planetary Debris Around Young White Dwarfs, Astronomy and Astrophysics 566 (2014)20. https://doi.org/10.1051/0004-6361/201423691

[5] Cs. Kiss, A. Mor, L.V. Tth, Far-infrared Loops in the 2nd Galactic Quadrant, Astronomy & Astrophysics 418 (2004) 131-141. https://doi.org/10.1051/0004-6361:20034530.

[6] V. Koenyves, Cs. Kiss, A. Moor, Z.T. Kiss, L.V. Toth, Catalogue of Far-infrared Loops in the Galaxy, A&A 463 (2007) 1227-1234. https://doi.org/10.1051/00046361:20065438

[7] R. Weinberger, and B. Armsdorfer, A Pair of 9 ° Long Dust Jets Ejected from Evolved Stars, Astronomical Society of the Pacific 313 (2004) 299.

[8] B. Aryal, C. Rajbahak, R. Weinberger, A Giant Dusty Bipolar Structure Around the Planetary Nebula NGC1514, Monthly Notices of the Royal Astronomical Society, 402 (2010) 1307-1312. https://doi.org/10.1111/j.1365-2966.2009.15966.x

[9] A. K. Jha, B. Aryal, Dust Color Temperature Distribution of Two FIR Cavities at IRIS and AKARI Maps, Journal of Astronomy and Astrophysics 39 (2018) 7. https://doi.org/10.1007/s12036-018-9517-6

[10] S.L. Schnee, N.A. Ridge, A.A. Goodman, G. L. Jason, A Complete Look at The Use of IRAS Emission Maps to Estimate Extinction and Dust Temperature, Astrophysical Journal 634 (2005) 442-450.

[11] X. Dupac, J.P. Bernard, N. Boudet, M. Giard, J.M. Lamarre, C. M"eny, F. Pajot, I. Ristorcelli, G. Serra, B. Stepnik, and J.P. Torre, Inverse Temperature Dependence of the Dust Sub-millimeter Spectral Index, Astronomy & Astrophysics 404 (2003) L11-L15. https://doi.org/10.1051/0004-6361:20030575

[12] D.O.S. Wood, P.C. Myers and D.A. Daugherty, IRAS Images of Nearby Dark Clouds, ApJS 95 (1994) 457-501. https://doi.org/10.1086/192107

[13] A.K. Jha, B. Aryal, A Study of a Cavity Nearby a Pulsar at -60º Latitude in the Far Infrared Map , JNPS 4(1) (2017) 33-41.

[14] A.K. Jha, B. Aryal, and R. Weinberger, A Study of Dust Color Temperature and Dust Mass Distributions of Four Far Infrared Loops, Revista Mexicana de Astronomia y astrofisica 53 (2017) 467-476.

[15] K. Young, T.G. Phillips, G.R. Knapp, Circumstellar Shells resolved in IRAS Survey data II-Analysis, Astrophysical Journal 409 (1993) 725-738. https://doi.org10.1086/172702

[16] A.K. Jha, B. Aryal, A Study of a Pulsar Wind Driven Structure in Far-infrared IRAS Map at Latitude -10º, JIST 22(1) (2017) 1-9.

[17] R.H. Hildebrand, The Determination of Cloud Masses and Dust Characteristics from Sub-millimeter Thermal Emission, Quarterly Journal of Royal Astronomical Society 24 (1983) 267-282.

[18] http://skyview.gsfc.nasa.gov/current/cgi/query.pl (2017).

[19] A.K. Jha, B. Aryal, A Study of Far- infrared Loop at -5º Galactic Latitude Around Pulsar J1627-5547, BIBECHANA 15 (2018) 70-76. https://doi.org/10.3126/bibechana.v15i0.18443